Inorganic Chemistry

pubs.acs.org/IC Article

Computationally Guided Investigation of the Optical Spectra of Pure β-UO_3

Tyler L. Spano,* Ashley E. Shields, Brianna S. Barth, Jeremiah D. Gruidl, Jennifer L. Niedziela, Roger J. Kapsimalis, and Andrew Miskowiec

Cite This: https://dx.doi.org/10.1021/acs.inorgchem.0c01279 Read Online

ACCESS | Metrics & More | Article Recommendations | Supporting Information

ABSTRACT: Single-phase β-UO_3 is synthesized by flash heating $UO_2(NO_3)\cdot 6H_2O$ in air to 450 °C and annealing for 60 h under the same conditions. For the first time, we report the Raman spectra of pure β-UO_3. To facilitate the assignment of Raman and infrared vibrational modes, we use density functional theory with density functional perturbation theory. By employing a novel analysis scheme that includes the mode frequencies as well as a quantitative analysis of the mode eigenvectors, we assign the observed spectral features to individual chemical modes. In particular, the density functional theory optimized structure, observed Raman spectrum, and eigenvector analysis suggest the presence of four crystallographically distinct uranyl ions, one more than has previously been suggested.

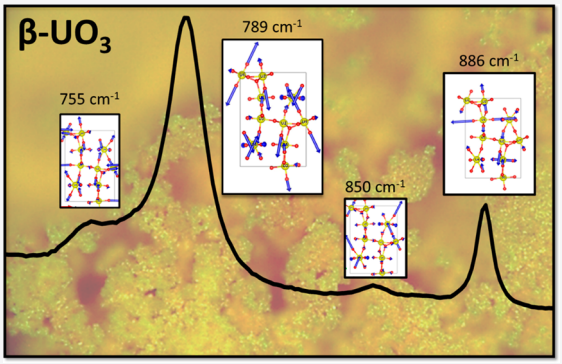

1. INTRODUCTION

1.1. Importance of the UO_3 Polymorphs. Uranium trioxide (UO_3) polymorphs have been the subject of numerous experimental and computational investigations because of their importance as intermediate materials in the nuclear fuel cycle.[1−4] Hydrolysis and calcination products of polymorphs within the UO_3 phase space were extensively explored in the mid-20th century.[5−7] Recently, the UO_3 system has garnered significant attention in the nuclear forensics community. Advances in Raman spectroscopy, including the development of hand-held, rapidly deployable systems as a means to determine major and impurity constituents in a sample, as well as the provenance of uranium ores, ore concentrates, and their derivatives have necessitated a renewed interest in the rapid identification of nuclear materials.[2,8−12] Raman spectra for other UO_3 polymorphs—including α, γ, and an amorphous phase—have been obtained, yet difficulties associated with the synthesis of pure β-UO_3 in recent years have precluded collection of vibrational spectroscopic data without contributions from other UO_3 phases, thus emphasizing the necessity of identifying this polymorph in a mixture.[13]

The present work has three goals: (1) to provide a facile and reliable method for obtaining pure β-UO_3 subsequent to a review of known synthetic routes, (2) to report the Raman spectra for β-UO_3, which has not been presented in pure form, and (3) to reevaluate the complex structure of β-UO_3 using experimental and computational methods and to relate the density functional theory (DFT) optimized structure to vibrational spectroscopic observables.

1.2. Reported Synthetic Routes. A variety of starting materials have been reported as precursors of β-UO_3. Hoekstra and Siegel[5] described a synthetic pathway involving the calcination of U_3O_8 in 40 atm of O_2 in the range of 500−550 °C or ignition of ammonium uranate or diuranate (ADU, $\sim(NH_4)_2U_2O_7$) in air to 500 °C, a method also reported by other researchers.[14,15] Wheeler et al. produced β-UO_3 as a product of rapidly heating (~35 °C/min) amorphous UO_3 hydrated in dilute NH_4OH.[16] Syntheses by Sato et al. described a mixture of β-UO_3 and U_3O_8 obtained by heating of $(NH_4)_2UO_4\cdot H_2O$.[17] Using ammonium uranyl nitrate as a precursor, Kim et al.[18] produced β-UO_3 in both air and N_2 by heating the starting material to 490 °C. Recently, Sweet et al. established a new synthetic pathway for β-UO_3 via calcination of ammonium uranyl carbonate ($(NH_4)_4UO_2(CO_3)_3$), which results in mixtures of amorphous and β-UO_3 or α- and β-UO_3 as a function of calcination temperature.[2]

To determine a reliable synthetic route for β-UO_3, the recent method of Sweet et al. was attempted as reported and with modifications to annealing conditions but, as those authors noted, the obtained product was a mixture of α- and β-UO_3 (Figure S1 in the Supporting Information).[2] ADU was also considered as a starting material on the basis of reports

Received: April 29, 2020

https://dx.doi.org/10.1021/acs.inorgchem.0c01279
Inorg. Chem. XXXX, XXX, XXX−XXX

from Debets,[19] Hoekstra and Siegel,[5] Wheeler et al.,[16] and Sato et al.,[17] who also investigated the thermal decomposition of UO_3 and ADU. Given the range of reported compositions for ADU in the literature and mixed-phase or low-quality reaction products obtained from this precursor material,[17,19,20] ADU was also deemed unsuitable for reliable syntheses.

Cornman[21] produced β-UO_3 by rapid calcination of uranyl nitrate hexahydrate (UNH, $UO_2(NO_3)_2{\cdot}6H_2O$) in air at 500 °C. A method similar to what Cornman used was recorded by Debets,[19] who investigated UNH as a precursor in addition to the ADU method described above. Debets found that the UNH starting material resulted in higher quality crystals[18] and was the first to provide crystal structure information for β-UO_3. Earlier works by Sheft et al.[7] and Katz and Gruen[22] did not provide structural information but described syntheses and reaction products similar to those discussed by Cornman and Debets. The successful synthesis of pure β-UO_3 from UNH in these early literature reports[19,21] and the commercial availability of this reagent indicated that UNH could be a promising starting material for the production of β-UO_3.

2. MATERIALS AND METHODS

Caution! Isotopically depleted uranium (^{238}U) was used in this synthesis following appropriate techniques and controls for handling radioactive materials.

2.1. Synthesis. Initially, UNH was heated to 500 °C at a rate of ∼35 °C/min followed by 72 h of annealing.[16,19] Powder X-ray diffraction (PXRD) and Raman spectroscopic data collected during annealing were used to monitor the reaction progress. Although this method produced an X-ray amorphous material, we observed some changes in the Raman spectra toward the end of the experiment (Figure S2 in the Supporting Information). We hypothesized that the maximum heating rate achievable during in situ experiments was insufficient to obtain β-UO_3 and modified this synthesis as discussed below.

Crystalline β-UO_3 was ultimately prepared by rapid calcination of UNH in air at 450 °C following the methods of Cornman[21] and Debets.[19] To promote homogeneous particle size distribution and even heating of the UNH precursor, 233 mg of $UO_2(NO_3){\cdot}6H_2O$ (Spectrum chemical, ACS grade) was ground in an agate mortar and pestle to break down the large crystals. UNH was placed in a porcelain crucible and then transferred in air to a Thermolyne muffle furnace preheated to 450 °C. The UNH was calcined at this temperature for 6 days, after which the furnace was brought to room temperature over 24 h. The crucible was removed from the oven, revealing a bright orange powder that was consistent with the reported appearance of β-UO_3.[13] This method was repeated with a smaller (∼25 mg) sample to ensure reproducibility, resulting in an identical product on the basis of PXRD.

2.2. Powder X-ray Diffraction. β-UO_3 was prepared for PXRD by grinding an approximately 50 mg subsample of the product described in section 2.1 in a mortar and pestle. The fine powder was loaded onto a zero-background Si substrate for PXRD analysis. Data were collected with a Proto AXRD benchtop powder diffractometer in Bragg−Brentano configuration with a Cu Kα (λ = 1.5406 Å) X-ray source and Dectris Mythen 1K 1-D detector. Incident and diffracted beam Soller slits and a 0.2 mm divergence slit were employed to reduce axial divergence. Data were collected in the range of 10−75° 2θ, with a step velocity of 0.06° 2θ/min. Before PXRD measurements, a zero alignment and analysis of instrumental broadening was conducted using LaB_6 standard reference material.

2.3. Scanning Electron Microscopy−Energy Dispersive X-ray Spectroscopy. Scanning electron microscopy−energy dispersive X-ray spectroscopy (SEM-EDS) analysis was conducted on several micrograms of β-UO_3 powder affixed to carbon tabs mounted on SEM stubs. Elemental analysis was conducted via EDS coupled to a Zeiss MERLIN field emission scanning electron microscope. An acceleration voltage of 10 kV and current of 1.1 nA was employed for EDS measurements at an 8−8.5 mm working distance. The sample morphology was examined using secondary and backscatter electron imaging with in-lens composite images.

2.4. Infrared Spectroscopy. Infrared spectra were collected using a ThermoFisher Scientific Nicolet iS5 attenuated total reflectance−Fourier transform infrared spectrometer (ATR-FTIR). Microgram subsamples of the powder were transferred to the diamond lens and were pressed using the ATR tip. Data were collected in the range of 650−1500 cm^{-1}. Background spectra, collected in air before the measurement of β-UO_3, were applied for baseline subtractions.

2.5. Raman Spectroscopy. A Renishaw inVia micro-Raman spectrometer was used to collect Raman data for the sample prepared as described in section 2.1. An excitation wavelength of 785 nm was used to collect spectra in the range of 35−1000 cm^{-1} in combination with a 1200 lines/mm diffraction grating, resulting in a resolution of ∼2.5−3.1 cm^{-1}. With the 532 nm laser, data were collected in the range of 100−1000 cm^{-1} with a 2400 lines/mm diffraction grating, resulting in a resolution of ∼0.80−1.01 cm^{-1}. A holographic notch filter provided spectral sensitivity to 35 cm^{-1} with the 785 nm laser. The corresponding power densities for both measurements were approximately 100 W/cm^2 on the basis of laser power (10 mW) and spot size (∼1 μm). Reported spectra from the 785 nm laser are the sum of 20 accumulations, each with a 10 s exposure time. Longer exposure times were used when collecting spectra with the 532 nm laser, with 30 accumulations of 20 s of data.

The high-energy region (650 cm^{-1} and above) of the Raman spectrum of β-UO_3 was analyzed using the Levenberg−Marquardt nonlinear least-squares method in the OriginPro2020 suite. First, background corrections were completed using an asymmetric least-squares method modeled after Eilers and Boelens.[23] Several models were then examined and compared using the Akaike information criterion.[24] Gaussian, Voigt, and pseudo-Voigt peak shapes were explored, and the number of peaks included in the fit was varied. On the basis of the Akaike information criterion, the best model resulted from fitting the experimental room-temperature data with six pseudo-Voigt peaks.

2.6. Computational Methods. Geometry optimization of the experimentally determined structure of Debets (Inorganic Crystal Structure Database Collection Code 14314) and phonon mode calculations were completed with the Vienna ab initio Simulation Package (VASP) using the generalized gradient approximation (GGA)[25−28] and the modified exchange-correlation functional of Perdew, Burke, and Ernzerhof revised for solids (PBEsol).[29] From Debets' structure, all lattice parameters and ionic positions were allowed to fully relax. For the geometry optimization, the calculations were allowed to proceed self-consistently via the conjugate gradient method with the ionic relaxation proceeding until the Hellmann−Feynman forces were converged to 10^{-3} eV A^{-1} and the electronic relaxation proceeding until the total energy converged to 10^{-8} eV/atom.

Interaction of the core and valence shells was described by the projector augmented wave method, and integration over the Brillouin zone was performed with the tetrahedron method as described by Blöchl.[30] A cutoff energy of 600 eV was used for the plane wave basis set along with a Γ-centered k-point mesh with 0.4 $Å^{-1}$ spacing in the Brillouin zone, after both were carefully checked for convergence. The effective Hubbard Hamiltonian approach of Dudarev et al., U_{eff}, was applied to the f electrons on uranium as a correction for the strong correlation of these electrons, with a value of U_{eff} = 4 eV.[31]

$$E_{GGA+U} = E_{GGA} + \frac{U-J}{2}\sum_{\sigma}\mathrm{Tr}[\rho^{\sigma} - \rho^{\sigma}\rho^{\sigma}] \quad (1)$$

where the parameters U and J are elements of the spherically averaged matrix of the screened Coulomb interaction and can be applied in VASP as $U_{eff} = U - J$. ρ^{σ} is the density matrix. Owing to the relatively large size of the β-UO_3 unit cell, a single unit cell was used for the

https://dx.doi.org/10.1021/acs.inorgchem.0c01279
Inorg. Chem. XXXX, XXX, XXX−XXX

density functional perturbation theory (DFPT) calculations. Post-processing was performed using the Phonopy Python package.[32]

3. RESULTS AND DISCUSSION

3.1. Powder X-ray Diffraction and Scanning Electron Microscopy. β-UO_3 was identified using the International Centre for Diffraction Data Powder Diffraction File 4+ (PDF Card 00-022-1079, Figure 1).[19] The powder pattern of β-UO_3

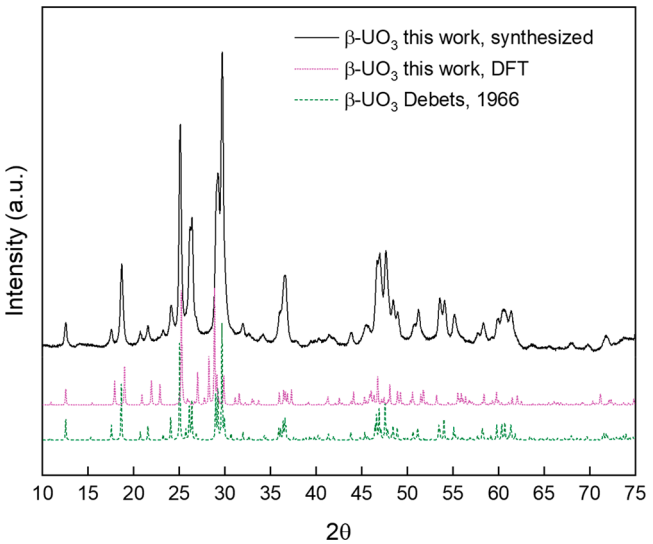

Figure 1. Powder X-ray diffractogram (Cu Kα, λ = 1.5406 Å) for β-UO_3 in comparison with the simulated powder pattern for Debets's β-UO_3 structure and the results of geometry optimization by DFT.

possesses sharp Bragg peaks with no reflection contributions from impurity phases. Some reflection broadening resulting from small crystallite domains is observed. The results of a Scherrer analysis of the 10 most intense reflections indicate an average crystallite size of 40.5 nm.[33]

The EXPO2014 software package was used to calculate lattice parameters and determine the space group of β-UO_3.[34] The results of autoindexing and space group determination by N-TREOR and subsequent refinement of lattice parameters yield a = 4.025 Å, b = 10.302 Å, and c = 14.630 Å with β = 100.412° in $P2_1$ (R_{wp} = 6.576%).[35] These results are consistent with the experimental X-ray structure of Debets.[19] Both Debets and Brincat report the monoclinic space group $P2_1$ for β-UO_3; however, identical 0k0 with k odd systematic absences for both $P2_1$ and $P2_1/m$ preclude ruling out the higher symmetry space group.[3] To examine the possibility of missed symmetry in the assigned space group of β-UO_3, crystallographic data provided by Debets was loaded into the PLATON software package, and the ADDSYM command was executed to check for additional symmetry and/or pseudosymmetry.[36] No additional symmetry elements were observed using this method, but the cell provided by Debets was found to be in a nonstandard setting (e.g., basis vectors oriented relative to symmetry elements rather than the smallest unit cell). The transformation matrix for converting to the reduced cell (a = 3.91 Å, b = 10.34 Å, c = 14.33 Å, β = 99.03°, Z = 10) is included in Table S1 in the Supporting Information.

Images of β-UO_3 collected using optical microscopy reveal a bright orange cryptocrystalline powder with a vitreous luster (Figure 2a). Secondary electron images show a massive anhedral to subhedral morphology with radiating micaceous

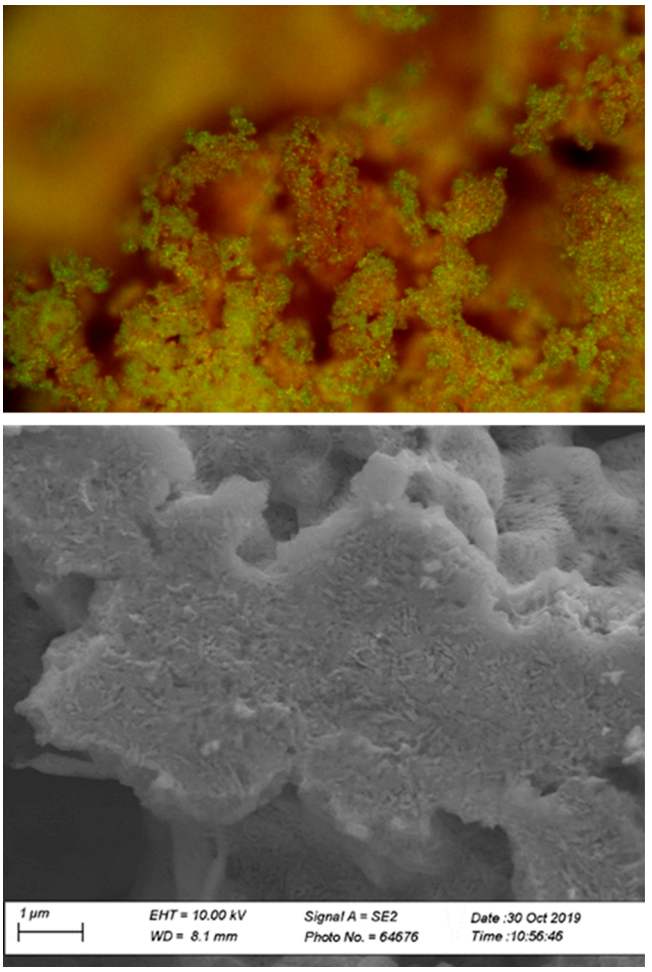

Figure 2. (a) Optical image of β-UO_3, which forms a bright orange cryptocrystalline powder with a vitreous luster. The field of view is 300 μm. (b) Secondary electron image of β-UO_3, which displays a massive anhedral to subhedral morphology with radiating micaceous crystallites that are approximately 200 nm in length.

crystallites that are approximately 200 nm in length (Figure 2b). Other notable morphological features include several areas possessing a botryoidal habit and areas of voids and vesicles likely resulting from rapid calcination (Figure S3 in the Supporting Information). SEM-EDS measurements indicate that only U and O are present in β-UO_3 (Figure S4 in the Supporting Information).

3.2. Computational Results. According to X-ray crystallographic results from Debets, β-UO_3 crystallizes in the monoclinic space group $P2_1$ with lattice parameters a = 10.34 Å, b = 14.33 Å, c = 3.91 Å, β = 99.03°, and Z = 10.[19] In Debets's structure (Figures 3 and 4), five unique U sites are described for β-UO_3, two of which are coordinated pseudoequatorially by five oxygen atoms and possess extremely bent uranyl-like oxygens (Figure 4a,b) forming distorted-pentagonal-bipyramidal coordination geometries. An additional U environment in β-UO_3 is, according to Debets, devoid of an -yl group, with one U site coordinated by six O atoms forming a distorted octahedron (Figure 4c). Two additional U sites were observed, decorated again nearly equatorially by four O nearest neighbors, resulting in distorted-square-bipyramidal coordination environments (Figure 4d,e).[19]

https://dx.doi.org/10.1021/acs.inorgchem.0c01279
Inorg. Chem. XXXX, XXX, XXX−XXX

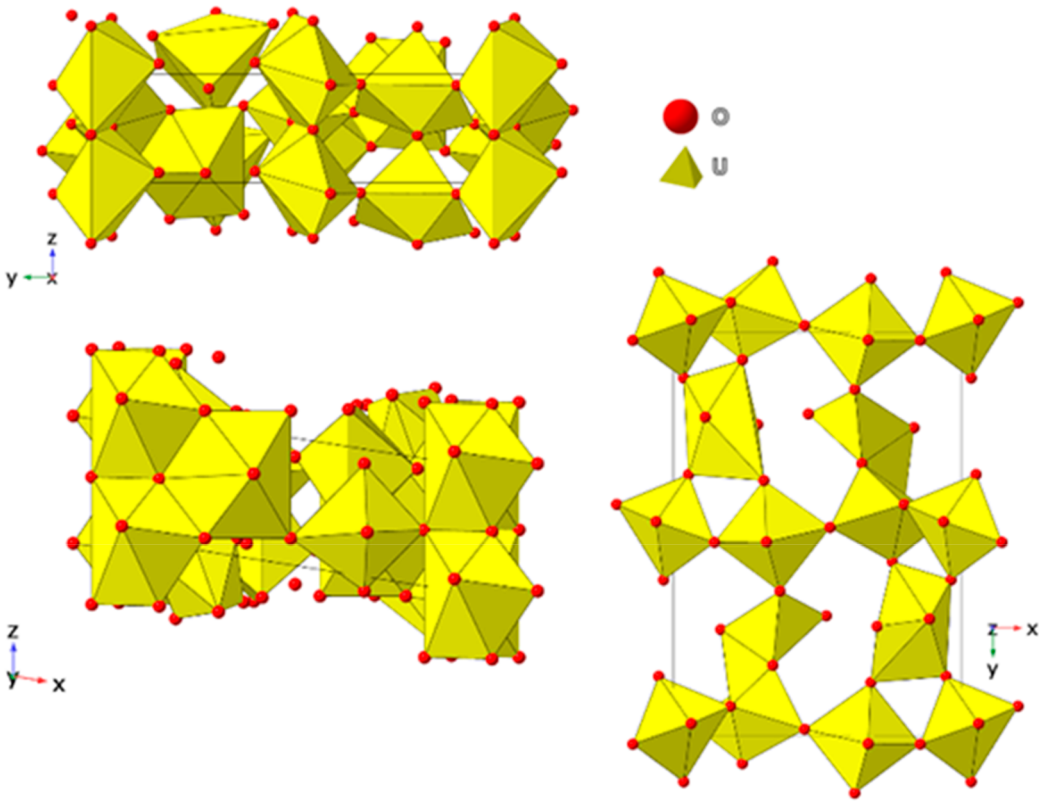

Figure 3. X-ray crystallographic structure of β-UO_3 solved by Debets in 1966.[19]

Brincat et al.[3] recently reexamined the structures of several uranium oxides, including β-UO_3, using DFT+U within the GGA with the PBE functional, with U and J values of 4.5 and 0.54 eV, respectively. Their results found U−O distances (∼1.6−1.9 Å) consistent with uranyl bonds,[3,37] but these authors state that the nonlinearity of "axial" O about these U centers preclude the formation of true uranyl units. Brincat et al. confirm that one U center possesses distorted-octahedral coordination and the remaining U sites have irregular 7-fold coordination, like the distorted-pentagonal-bipyramidal geometry described for U1 and U2 in the experimental structure (Figure 4a,b).

Our geometry optimization of the β-UO_3 structure by DFT confirms that additional uranyl centers are present (Figure 5 and Table 1). U1 and U2 remain in pentagonal-bipyramidal coordination but display increased linearity of O−U−O centers in comparison to the experimental structure of Debets (Figure 5a,b and Table 1). Furthermore, U−O_{yl} bond distances of the U2 center in our DFT-optimized structure are more consistent with reported values for this type of bond than was observed experimentally.[37] In our optimized structure, U3 is also less distorted in octahedral coordination than this same center in the experimental structure of Debets, as evidenced by increased isotropy of the coordinating O with respect to U−O distances and O−U−O angles (Figure 5c). Upon geometry optimization, U4 remains in the same square-pyramidal geometry observed experimentally by Debets and computationally by Brincat but with longer and more linear U−O_{yl} bonds (Figure 5d and Table 1). For U5 (Figure 5e and Table 1), geometry optimization by DFT reveals a distorted-hexagonal-bipyramidal coordination environment, which was not seen in the experimental structure of Debets or in the DFT-optimized structure of Brincat et al. Differences between the coordination environments in Figure 5 and those determined by Brincat et al. are attributable to our use of the PBEsol functional, which has been shown to be a more appropriate model for actinide oxide systems in comparison to PBE.[38] Comparing optimizations resulting from additional calculations performed with both PBE and PBEsol confirm that the use of the PBE functional produces a structure very similar to that found by Brincat et al. Furthermore, use of the PBEsol functional more closely reproduced the experimental lattice parameters and enabled detection of an additional uranyl center.

In addition to axial U−O_{yl} bond lengths and angles for U1, U2, U4, and U5 in our DFT-optimized structure of β-UO_3, calculated ν_1 and ν_3 frequencies expected to result from these bonds in experimental IR and Raman spectra have been tabulated and are included in Table 1. Empirical relationships developed to relate U−O_{yl} distances to observed frequencies in vibrational spectra were applied to both experimental and computationally optimized bond lengths, following procedures described by Jones, Glebov, and Bartlett and Cooney.[39−41]

Group theory analysis based on symmetry indicates that the relaxed β-UO_3 structure possesses 120 unique vibrational modes, and all are Raman and IR active. Table S2 in the Supporting Information contains phonon frequencies calculated from DFPT, their irreducible character, and corresponding experimentally observed modes. Expected uranyl bond lengths calculated using the methods of Jones, Glebov, and Bartlett and Cooney described above are also included.

The phonon eigenvectors, $\mathbf{u}_i^n$, for each mode (indexed by n) describe the displacement of atoms (indexed by i) along the Cartesian axes at $\mathbf{Q} = \Gamma$. Since optical scattering occurs near Γ, the atomic displacements at the Γ point in the Brillouin zone describe the motion of atoms during inelastic light scattering.

https://dx.doi.org/10.1021/acs.inorgchem.0c01279
Inorg. Chem. XXXX, XXX, XXX−XXX

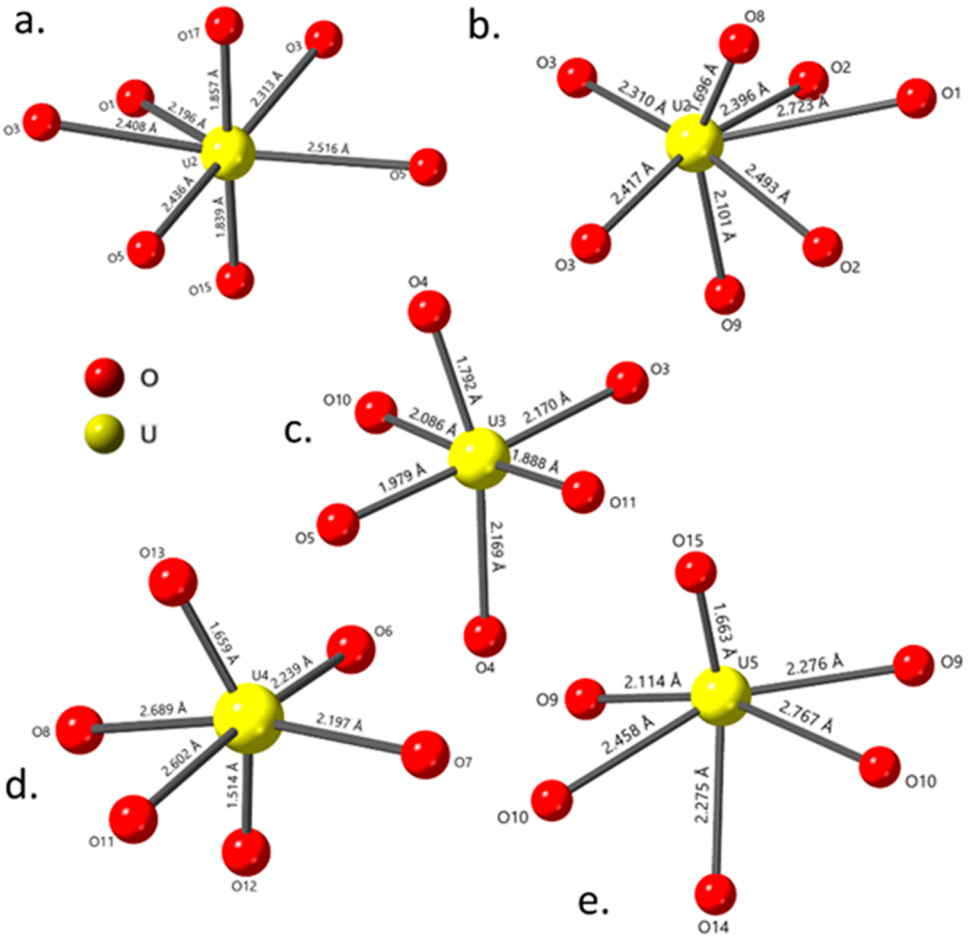

Figure 4. Coordination geometries of the five unique U sites in the structure of β-UO_3 as determined by Debets (1966): (a) U1 and (b) U2 in a distorted-pentagonal-bipyramidal coordination; (c) U3 in a distorted-octahedral coordination; (d) U4 and (e) U5 in a distorted-square-bipyramidal coordination.

Because the uncertainty of phonon frequencies calculated via DFT is high in comparison to the mode density in frequency space, especially in the uranyl region, employing an alternative method of mode identification to simple frequency matching is necessary. To do this, we calculate the fraction of atomic displacement amplitude associated with select atoms for each mode. For instance, in analyzing the motion of the U1 uranyl ion (Figure 5a), we form the set of atoms (yl_1 = [O13, O11, U1]) and their crystallographically equivalent sites, and calculate their amplitude sum:

$$s^n_{yl_1} = \sum_{i\epsilon[yl_1]} |\boldsymbol{u}^n_i| = \sum_{i\epsilon[yl_1]} \sqrt{(u^n_{i_x})^2 + (u^n_{i_y})^2 + (u^n_{i_z})^2}$$

The $s_{yl}{}^n$ values are normalized by total mode amplitude

$$s^n = s^n_{yl} / \sum_{i=1}^{N} |\boldsymbol{u}^n_i|$$

where N includes all atoms in the unit cell. Higher values of s^n indicate that a larger fraction of mode amplitude originates from motion of uranyl oxygen or uranium atoms (Table 2 and Table S3 in the Supporting Information). Using this method, it is possible to easily correlate Raman-active symmetric and infrared-active antisymmetric stretching modes of each uranyl ion by finding the largest values of s^n. This approach is especially useful for separating regions with multiple uranyl ion contributions that are difficult to distinguish by frequency alone. Furthermore, obtaining both the Raman and infrared frequencies on a per uranyl group basis allows the simultaneous attribution of multiple experimental optical bands to a single chemical moiety. To visualize these intensity contributions and confirm assignments, eigenvectors of each phonon mode have been plotted in VESTA over the relaxed structure to illustrate the motion of participating atoms (e.g., Figure 6a, 948 cm^{-1} phonon, and the Supporting Information).[32,42]

In addition, the eigenvector phase angle can be calculated for each uranyl group, j = 1−5, using the equation

$$\theta^n_j = \cos^{-1}\left(\frac{\boldsymbol{u}^n_{O_{yl1}} \cdot \boldsymbol{u}^n_{O_{yl2}}}{|\boldsymbol{u}^n_{O_{yl1}}||\boldsymbol{u}^n_{O_{yl2}}|}\right)$$

Angles near zero indicate collinear motion of uranyl oxygens, commensurate with an "antisymmetric" stretching mode, whereas angles near 180° indicate antilinear motion (out of phase). Because the β-UO_3 structure possesses relatively low symmetry, the phase angles for uranyl modes neither correspond precisely to zero and 180° nor do they indicate optical selection rules (Raman or infrared activeness), but the phase angles can be used to assist in determination of a qualitative character of each mode. For instance, eigenmodes with phase angles near 180° are the qualitative equivalent of

https://dx.doi.org/10.1021/acs.inorgchem.0c01279
Inorg. Chem. XXXX, XXX, XXX−XXX

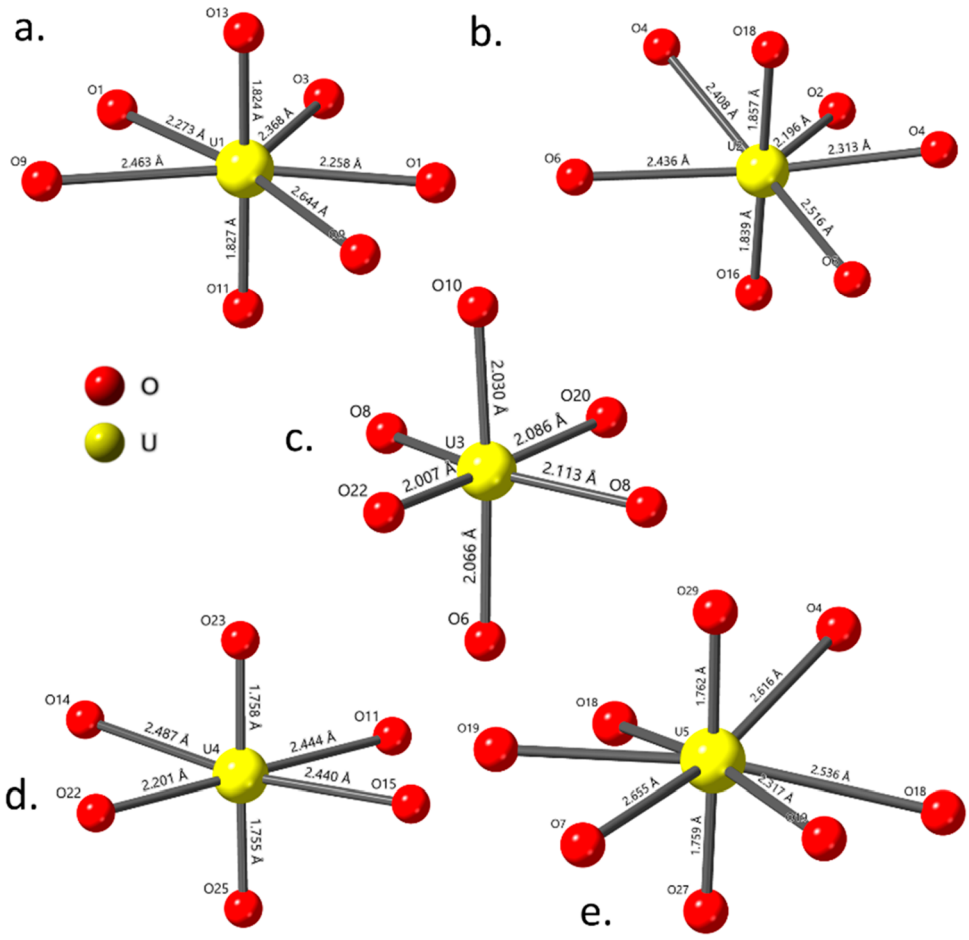

Figure 5. Uranium coordination environments in the DFT optimized structure of β-UO_3: (a) U1 and (b) U2 possessing a distorted-pentagonal-bipyramidal coordination geometry; (c) U3 remaining in octahedral coordination; (d) U4 possessing a square-bipyramidal coordination; (e) U5 showing a distorted-hexagonal-bipyramidal coordination geometry.

Table 1. Uranyl Bond Lengths and Angles from the X-ray Crystallographic Structure of Debets[19] Compared with Results of DFT Geometry Optimization[a]

	Oyl Distance (Å)		Uranyl Angle (°)		ν1 Frequency Calculated (cm^{-1})		ν3 Frequency Calculated (cm^{-1})	
U Center	Debets, 1966	DFT, this work	Debets, 1966	DFT, this work	Debets, 1966	DFT, this work	Debets, 1966	DFT, this work
U1	1.86	1.83	173.05	176.81	754.52	781.73	789.99	833.52
	1.84	1.82			772.48	791.17	818.57	848.93
U2	1.70	1.84	149.10	178.15	921.08	772.48	1078.37	818.57
	2.10	1.86			583.61	754.52	544.85	789.99
U4	1.70	1.76	152.15	175.24	921.08	852.01	1078.37	952.25
	1.51	1.76			1215.65	852.01	1742.45	952.25
U5	1.66	1.76	148.85	177.32	972.48	852.01	1178.80	952.25
	2.27	1.76			498.05	852.01	438.72	952.25

[a] ν_1 symmetric and ν_3 antisymmetric stretching frequencies calculated from experimental and DFT optimized uranyl bond lengths are also included.

Raman-active symmetric stretching modes (Table 2 and Table S3 in the Supporting Information). Moreover, although all modes are Raman active by symmetry, we do not expect to find significant Raman intensity in a mode with a small (but nonzero) phase angle that would indicate a particular mode is qualitatively similar to an antisymmetric, infrared-active mode.

3.3. Infrared Spectrum of β-UO_3. Infrared spectra collected for β-UO_3 are in good agreement with previously reported results[15,22,43] and are characterized by strong, well-defined absorbance bands at 966 and 911 cm^{-1} (Figure 7). The band located at 911 cm^{-1} in the experimental data is attributed to the $\nu_3(UO_2^{2+})$ antisymmetric stretching vibration on the basis of literature precedent.[5] This assignment is consistent with intensity contributions calculated using the method described in dection 3.2 (Table 2); however, a shift in frequency is observed for computational results (890 cm^{-1}, DFPT predicted frequency). This assignment is bolstered by further examination of Table 2, which indicates antisymmetric stretching in this region for U2. Eigenvectors associated with the 890 cm^{-1} phonon (Figure 6) confirm this, highlighting the advantage of using multiple methods to assign vibrational spectroscopic modes from DFPT results. Symmetric stretchings for U1, U3, U4, and U5 also occur at 890 cm^{-1}, but their contributions to intensity in the experimental IR are likely minimal (Table 2). Strong antisymmetric stretching of axial U1 and U2 O atoms is observed at 876 cm^{-1} and may also contribute to the observed intensity at 911 cm^{-1} (Figure 6 and Table 2).

https://dx.doi.org/10.1021/acs.inorgchem.0c01279
Inorg. Chem. XXXX, XXX, XXX−XXX

Table 2. Results of Atom Displacement and Phase Angle Calculations from DFPT Described in Section 3.2[a]

Contributing Center	U1		U2		U3		U4		U5	
Coordination	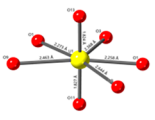		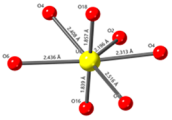		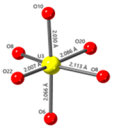		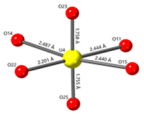		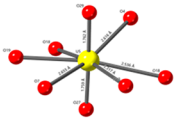	
Frequency (cm^{-1})	s^n	Angle	s^n	Angle	s^n	Angle	s^n	Angle	s^n	Angle
1038.93	0.02	121.17	0.03	122.13	0.02	10.01	0.44	1.51	0.45	2.16
1038.66	0.05	6.45	0.05	25.85	0.02	117.88	0.43	1.48	0.44	2.14
995.27	0.09	5.86	0.04	11.33	0.02	133.37	0.42	1.91	0.41	2.06
994.19	0.03	168.87	0.01	126.28	0.01	101.47	0.48	2.13	0.46	2.01
948.44	0.41	2.98	0.23	2.58	0.09	4.31	0.09	164.83	0.08	177.85
890.13	0.11	176.32	0.29	1.64	0.10	156.28	0.14	175.77	0.28	177.58
876.70	0.07	8.05	0.22	1.29	0.07	163.11	0.08	174.93	0.46	179.44
856.56	0.23	7.11	0.05	151.75	0.02	57.80	0.35	176.83	0.25	178.65
849.36	0.52	4.38	0.04	167.38	0.02	150.73	0.27	170.56	0.08	172.82
848.00	0.04	15.98	0.21	7.67	0.05	47.16	0.61	179.54	0.01	59.65
818.60	0.27	3.66	0.33	6.88	0.10	166.79	0.10	168.59	0.23	178.23
806.26	0.06	72.70	0.37	5.85	0.12	157.14	0.18	176.28	0.31	175.26
776.42	0.35	179.76	0.22	171.32	0.07	146.67	0.14	176.37	0.02	26.50
771.15	0.42	179.60	0.23	177.07	0.15	162.05	0.02	142.28	0.02	123.71
747.11	0.17	178.02	0.20	176.08	0.24	161.95	0.04	168.85	0.01	76.82
746.64	0.09	177.57	0.23	176.74	0.25	173.63	0.04	177.39	0.03	153.83
734.07	0.09	171.33	0.24	179.70	0.18	175.07	0.06	172.32	0.05	159.32
724.39	0.04	162.19	0.25	178.73	0.24	171.52	0.06	164.47	0.05	164.57
653.51	0.01	165.22	0.01	117.02	0.06	85.16	0.00	82.22	0.01	65.08
653.41	0.00	96.85	0.01	165.90	0.05	137.99	0.00	18.29	0.01	21.56
615.34	0.12	166.27	0.12	44.46	0.20	10.38	0.03	120.58	0.05	153.78

[a]Darker shading indicates greater U center contributions (s^n) and phase angles closer to 180°.

The higher energy mode at 966 cm^{-1} in the experimental IR spectrum was observed by other researchers.[43,44] Allen and Holmes[43] and Tsuboi et al.[45] allude to this as originating from an additional UO_2^{2+} stretching mode, but neither provided definitive evidence of this assignment. The experimentally observed absorption intensity coupled with crystallographic data from Debets[19] and our DFT results suggest that the hypotheses of Allen and Holmes[43] and Tsuboi et al.[45] are correct that this band originates from an additional $\nu_3(UO_2^{2+})$ mode from one (or more) of the five U centers in β-UO_3. An examination of Table 2 reveals that the computationally predicted mode at 948 cm^{-1} corresponds to antisymmetric polarization along the uranyl for U1, U2, and U3 with symmetric stretching contributions observed for U4 and U5. This DFPT-predicted phonon mode is approximately 18 cm^{-1} lower than what was observed experimentally and is a shift (~21 cm^{-1}) similar to what was predicted computationally (890 cm^{-1}) for the 911 cm^{-1} experimental mode (Table 2). Furthermore, antisymmetric stretching of axial oxygens is seen in the eigenvector visualization produced for this frequency (Figure 6 and the Supporting Information).

Weak absorptions located at ~885, 874, and 864 cm^{-1} in the experimental IR data (Figure 7) may also result from slight differences in coordination about the multiple U centers in β-UO_3. Like the band located at 966 cm^{-1}, these lower intensity absorptions likely originate from the $\nu_3(UO_2^{2+})$ antisymmetric stretching vibrations of additional U−O_{yl} bonds. Evidence supporting this hypothesis is that reasonable U−O_{yl} bond lengths (1.76−1.8 Å) are obtained when they are calculated from the experimental IR spectra using the method of Glebov discussed in section 3.2,[41] with the assumption that modes at 885, 874, and 864 cm^{-1} originate from $\nu_3(UO_2^{2+})$ stretching vibrations. The range of calculated bond distances is also in excellent agreement with uranyl bond lengths in the DFT-optimized structure (Table 1 and Figure 5). Further justification is provided by an examination of Table 2 and eigenvectors associated with these modes. Significant antisymmetric stretching of axial oxygens is predicted for U1 and U2 at 876 cm^{-1}. Similarly, at 856, 849, and 848 cm^{-1}, antisymmetric stretching of axial O associated with U1, U2, and a combination thereof is observed (Table 2 and Table S3 in the Supporting Information). Although there are some differences between theory and experiment, such as a slight shifting that occurs for predicted vibrational modes (Table 2) relative to what is observed experimentally (Figure 7), the complexity resulting from multiple U coordination environments in the structure of β-UO_3 is clearly manifested in the high-energy region of the IR spectrum.

Complicated absorption behavior is also observed in the range of ~800−650 cm^{-1} with bands centered at 802, 783, 746, 724, 689, and 666 cm^{-1} (Figure 7). DFPT predicts numerous phonons in this region (Table 2 and Table S2 in the Supporting Information). Khilla et al. provide a comparison of IR spectra for the UO_3 polymorphs and attribute vibrational modes in the range of 660−790 nm to equatorial U−O stretching. Again, given the numerous U coordination environments in the experimental and computationally optimized structures of β-UO_3, this assignment by Khilla et al. is likely correct.[3,15,19] As seen in Table 2 and Table S3 in the Supporting Information, fewer uranyl contributions are present here in comparison to the higher energy (>800 cm^{-1}) region of the IR spectrum. Phonon eigenvector illustrations show that stretching of equatorial oxygens about U4 and U5 centers is occurring at 806 cm^{-1} (Supporting Information), but Table 2 indicates that antisymmetric uranyl stretching for U2 arises at the same frequency and thus may be contributing to the observed absorption intensity. Likewise, predicted modes in Table 2 and an examination of phonon eigenvectors suggest

https://dx.doi.org/10.1021/acs.inorgchem.0c01279
Inorg. Chem. XXXX, XXX, XXX−XXX

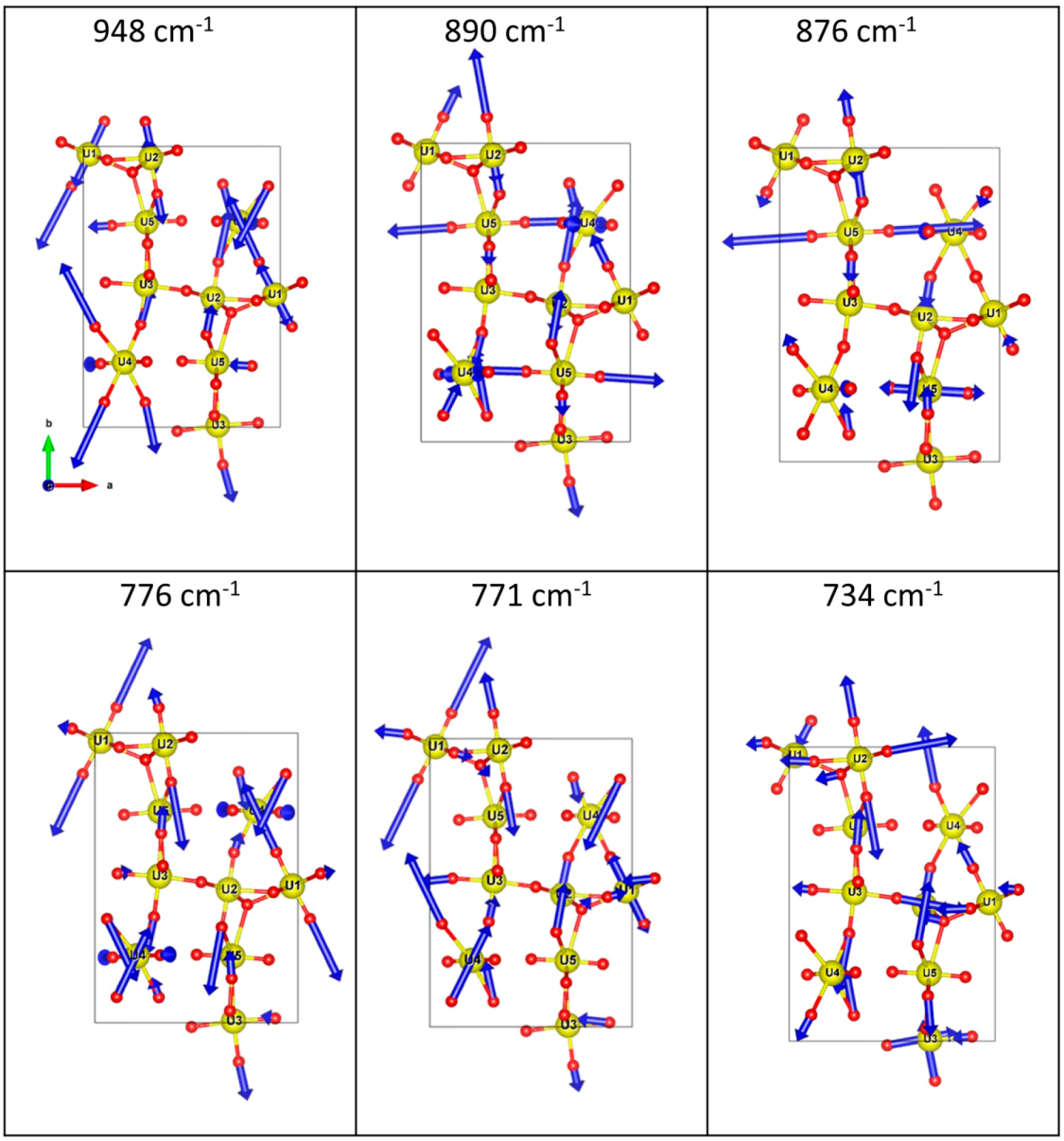

Figure 6. Phonon eigenvector visualizations for select vibrational modes predicted from DFPT.

that the mode at 776 cm^{-1} is composed of intensity contributions from U5 antisymmetric stretching coupled with equatorial O about U4. Equatorial O vibrations are also seen at 771 cm^{-1} for U4 and U5 on the basis of phonon eigenvector visualizations (Supporting Information). High-magnitude symmetric stretching is also observed for all U centers in this region (~720−780 cm^{-1}, Table 2), which is expected to manifest intensity at approximately the same frequency in the experimental Raman spectrum of β-UO_3 (section 3.4 and Figure 8). Table 2 shows that symmetric uranyl stretching is present in this region, but eigenvector visualizations indicate that equatorial O vibrations about U1, U2, U4, and U5 centers are also occurring at this frequency (Supporting Information), highlighting the importance of using visualizations (e.g., Figure 6) and calculations (Table 2) in tandem to assign vibrational spectra on the basis of DFPT results.

3.4. Raman Spectrum of β-UO_3. The Raman spectrum of β-UO_3 is dominated by an intense vibrational mode at 789 cm^{-1} central to an apparent quintet of modes in the range of 650−900 cm^{-1} (Figure 8). Deconvolution of this region as described in section 2.5 reveals additional complexity, with six peaks contributing to observed intensities (Table S2 in the Supporting Information). As with other U compounds possessing U(VI) in the linear -yl configuration, uranyl symmetric stretching vibrations are prevalent here.[46] Similar to observations from IR spectroscopy, the varying intensity and complexity of vibrational modes in this region can be attributed to the five symmetrically unique U sites in β-UO_3. To this end, the center of each mode obtained from the peak fitting procedure described in section 2.5 was applied to the empirical relationship described by Bartlett and Cooney[40] discussed in section 3.2 to calculate uranyl distances (Table S2 in the Supporting Information). Additionally, as was done for IR data in section 3.3, uranyl-related stretches documented in Table 2 and eigenvector visualizations like those shown in Figure 6 were used to guide mode assignments for the experimental Raman spectra shown in Figure 8.

https://dx.doi.org/10.1021/acs.inorgchem.0c01279
Inorg. Chem. XXXX, XXX, XXX−XXX

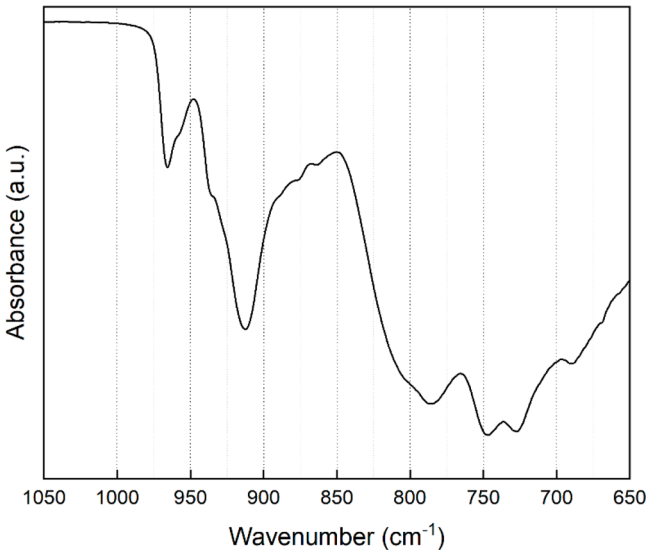

Figure 7. Infrared spectrum of β-UO_3. Strong absorbance bands are observed at 966 and 911 cm^{-1} and correspond to $\nu_3(UO_2^{2+})$ asymmetric stretching vibrations. Vibrational modes associated with equatorial U−O are visible in the lower energy (<800 cm^{-1}) region.

Bond length calculations for vibrational modes in the range of 700−900 cm^{-1} completed using the method of Bartlett and Cooney[40] indicate that uranyl bonds range from 1.92 Å (702 cm^{-1} mode) to 1.73 Å (887 cm^{-1} mode) (Table S2 in the Supporting Information). These distances are consistent with U−O_{yl} lengths in the experimental crystal structure of Debets and with our DFT results[19] (Figures 4 and 5 and Table 1). Similar to results from IR spectroscopy, these bond lengths indicate the presence of additional uranyl-type centers in β-UO_3. The emergence of uranyl bonds is further evidenced by nearly linear (176.8−178.1°) angles calculated for all U centers and coordinating O with distances of ∼1.8 Å (Table 1).

To validate the bond lengths calculated from experimental spectra and to more definitively assign uranyl peaks, the frequencies of phonon modes obtained from DFPT (Table S2 in the Supporting Information) were also used to calculate expected uranyl bond lengths, again using the method of Bartlett and Cooney[40] (Table S2 in the Supporting Information). In tandem with results included in Table 1 and eigenvector visualizations like those in Figure 6, Raman peaks located at ∼770, 788, 851, and 886 cm^{-1} in the experimental data were assigned to the stretching modes of individual U coordination environments or combinations thereof.

Applying these cross validations to the highest intensity vibrational mode in the experimental Raman spectra leads to the assignment of the band centered at 788 cm^{-1} to the $\nu_1(UO_2^{2+})$ symmetric stretching vibration, composed primarily of contributions from axial O of the U1 center. According to DFPT results, symmetric stretching of axial oxygens about the U1 center with additional contributions from U2−O and, to a lesser extent, U4−O stretching (Table 2) occurs at 776 cm^{-1}. Similarly, at 771 cm^{-1}, Table 2 indicates that intense symmetric stretching of O about U1 and U2 occurs, with small uranyl contributions at all other U sites. In addition to the intensity contributions indicated in Table 2, eigenvector visualization of the 776 and 771 cm^{-1} phonons shows symmetric uranyl stretching at these frequencies (Figure 6). As further justification for this assignment, the U−O_{yl} bond

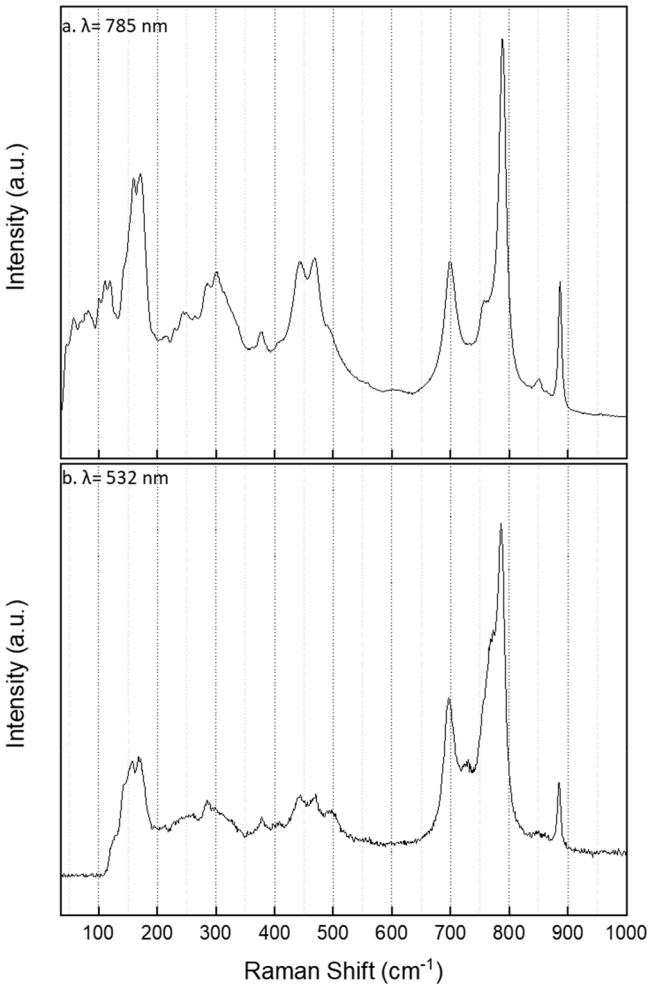

Figure 8. Raman spectrum of β-UO_3 collected with (top) 785 nm and (bottom) 532 nm excitation wavelengths. The intense peak at 788 cm^{-1} is attributed to symmetric stretching of uranyl oxygens associated with U1. Peak centers obtained from fitting data in (a) as described in section 2.5 are included in Table S2 in the Supporting Information for reference.

length expected to produce this frequency as calculated from the experimental spectra is 1.82 Å. A similar bond length is derived from computationally predicted phonon frequencies (771 cm^{-1}, 776 cm^{-1}, and 1.84 Å; Table S2 in the Supporting Information). Furthermore, U1−O13 and U1−O11 (1.82 and 1.83 Å, respectively; Figure 6a and Table 1) bond distances observed in the DFT-optimized structure are in good agreement with uranyl bond lengths predicted from both the experimental data and the DFPT phonons (Table S2 in the Supporting Information).

A low-intensity shoulder peak composed of intensity contributions from the $\nu_1(UO_2^{2+})$ symmetric stretching of axial oxygens about U1 and U2 centers, with lesser contributions from other U centers (Table S3 in the Supporting Information), is located at ∼770 cm^{-1} in the experimental Raman data (∼750 cm^{-1} DFPT predicted). Eigenvector illustrations for these frequencies and the expected U−O_{yl} bond length calculated from the position of this experimental mode (1.86 Å) confirm this assignment and suggest that a larger portion of the observed intensity originates from U2 O. Furthermore, the predicted position (754 cm^{-1}) of the $\nu_1(UO_2^{2+})$ mode calculated from the bond

https://dx.doi.org/10.1021/acs.inorgchem.0c01279
Inorg. Chem. XXXX, XXX, XXX−XXX

distance (U2−O18, 1.86 Å) in the DFT-optimized structure is in excellent agreement with the experimental spectra (Table 1). Table 2, Table S2 in the Supporting Information, and the eigenvector visualization (Supporting Information) also indicates that some polarization of O−U3−O occurs in this region. Therefore, symmetric stretching of O about U3 in octahedral coordination may also be contributing to the experimentally observed intensity at ∼770 cm^{-1}.

A lower intensity mode located at ∼730 cm^{-1} in the deconvoluted experimental data originates from the $\nu_1(UO_2^{2+})$ symmetric stretching of oxygens about the U2, U3, and, to a lesser extent, U1 centers on the basis of the results in Table 2. From the Bartlett and Cooney relationship, this mode corresponds to a uranyl bond length of 1.88 Å (Table S2 in the Supporting Information), such as the longer uranyl bond lengths seen for U2 in the DFT-optimized structure (Figure 5 and Table 1). Examination of the eigenvectors associated with this frequency again highlights the need for multiple validation methods in assigning experimental Raman spectra on the basis of computational results. Visual analysis alone suggests symmetric and antisymmetric stretching for U2−O and U3−O, respectively, in the 734 cm^{-1} phonon mode (Figure 6), whereas the results in Table 2 indicate that symmetric O stretching is predicted at this frequency for both centers.

On the basis of 1.76 Å $U-O_{yl}$ bond lengths for U4 and U5 in the DFT-optimized structure (Table 1 and Figure 5d,e), these centers are expected to manifest a symmetric stretching vibrational mode centered at ∼850 cm^{-1} in experimental Raman spectra, which is indeed observed in Figure 8a. Table 2 also indicates that the intensity here is largely composed of symmetric uranyl stretching associated with U4 (predicted at 848 cm^{-1}). Symmetric stretchings of axial O for U4 and U5 are also seen in the eigenvectors associated with modes in this region (Supporting Information), again emphasizing the need for multiple methods of assigning Raman spectra.

In addition to complex uranyl modes in the high-energy region, a doublet of peaks with both high- and low-energy shoulders in the range of 450−470 cm^{-1} is observed (Figure 8). These features were observed by Sweet et al. in the calcination products of $(NH_4)_4UO_2(CO_3)_3$, which were a mix of amorphous and β-UO_3, but no assignments were provided by these authors.[47] Deconvolution of spectral features in this range as described in section 2.5 indicates that at least four unique peaks are contributing to the observed intensity. Although these modes may be combination bands resulting from the multiplicity of features in the low-energy (ca. 100−300 cm^{-1}) region of the spectra, Table S3 in the Supporting Information indicates that uranyl contributions to intensity persist through this lower energy region, to approximately 461 cm^{-1}. Significant motion of O coordinating the U3 center (in distorted-octahedral coordination) is also observed in this region with additional intensity contributions from U1 and U5 equatorial O vibrations (Table S3 in the Supporting Information, ∼ 460 cm^{-1} phonon eigenvectors).

The results of peak fitting suggest that as many as 28 individual modes contribute to the observed intensities in the low-energy region between 35 and 400 cm^{-1}. Low intensity and high complexity here may be attributed to the appearance of multiple uranyl and equatorial O modes originating once again from the distinct coordination environments at each crystallographically unique U site (Figure 5).[48] Confirming this assessment, numerous phonon modes are predicted in this region (Table S2 in the Supporting Information). Eigenvector visualizations associated with DFPT predicted modes (see the Supporting Information) in the range of 38−78 cm^{-1} show that only low-magnitude lattice vibrations are occurring here. At ∼81 and 86 cm^{-1}, however, intensity contributions from O coordinating U3 are suggested upon examination of eigenvector images (see the Supporting Information). Lattice vibrations similarly dominate the region of ∼90−136 cm^{-1}, after which equatorial modes originating from all U centers and combinations thereof are realized in the ∼145−400 cm^{-1} phonons (see the Supporting Information).

The complex Raman spectrum of β-UO_3 is contrasted by simple spectra observed for amorphous and α- and γ-UO_3.[2,4,8,49,50] The structures of α- and γ-UO_3 contain only one unique U coordination environment,[51,52] whereas the multiple uranyl centers observed in β-UO_3 produce the complicated spectrum seen in Figure 8. Amorphous UO_3 is characterized by a diffuse Raman peak centered at ∼692 cm^{-1}, with low-intensity shoulders at 758 and 865 cm^{-1}.[52] Raman spectra for α-UO_3 show only two peaks in the range of 600−1000 cm^{-1}, centered at 760 and 830 cm^{-1}.[4] Similarly, the Raman spectrum for γ-UO_3 is characterized by peaks centered at 767 and ∼840 cm^{-1}.[2,8] No other vibrational modes are observed in the range of 600−1000 cm^{-1} for γ-UO_3, which is in contrast to the six peaks seen in this region for β-UO_3. The complex structure and, subsequently, Raman spectrum of β-UO_3 results in it being readily distinguished from the other polymorphs using micro-Raman spectroscopy.

4. CONCLUSIONS

Pure β-UO_3 has been synthesized by the facile calcination of uranyl nitrate in air following a review of the reported synthetic routes. PXRD and SEM-EDS were used to characterize β-UO_3 and indicate that a pure and homogeneous product was obtained. IR spectra of β-UO_3 are in good agreement with previously reported results. The Raman spectrum of pure β-UO_3 is presented for the first time, including the low-energy region (35−100 cm^{-1}). DFT and DFPT calculations were used to optimize the structure of and calculate phonon modes for β-UO_3. DFT geometry optimization and experimental results confirm that four U centers (U1, U2, U4, and U5) in β-UO_3 possess the UO_2^{2+} uranyl unit. U1 and U2 are decorated by five O atoms in the equatorial plane, resulting in distorted-pentagonal-bipyramidal coordination, whereas U4 and U5 are characterized by square- and hexagonal-bipyramidal geometries, respectively. Finally, the results of DFPT calculations enabled assignment of uranyl vibrational modes in the experimental IR and Raman spectra of β-UO_3.

■ ASSOCIATED CONTENT

Supporting Information

The Supporting Information is available free of charge at https://pubs.acs.org/doi/10.1021/acs.inorgchem.0c01279.

Eigenvector visualization files of the DFT optimized structure of β-UO_3 (ZIP)

Powder X-ray diffraction and Raman spectroscopic data from preliminary syntheses performed in this work, additional SEM-EDS images and data, transformation matrix for converting the reported cell of β-UO_3 to a standard setting, a complete tabulation of DFPT-predicted phonon modes with corresponding results from experimental Raman spectra, and detailed results of analyses described in section 3.2 (PDF)

https://dx.doi.org/10.1021/acs.inorgchem.0c01279
Inorg. Chem. XXXX, XXX, XXX−XXX

AUTHOR INFORMATION

Corresponding Author

Tyler L. Spano − *Nuclear Nonproliferation Division, Oak Ridge National Laboratory, Oak Ridge, Tennessee 37831, United States;* orcid.org/0000-0001-6572-9722; Email: spanotl@ornl.gov

Authors

Ashley E. Shields − *Nuclear Nonproliferation Division, Oak Ridge National Laboratory, Oak Ridge, Tennessee 37831, United States*

Brianna S. Barth − *Nuclear Nonproliferation Division, Oak Ridge National Laboratory, Oak Ridge, Tennessee 37831, United States; University of Texas at Austin, Department of Chemistry, Austin, Texas 78712, United States*

Jeremiah D. Gruidl − *Nuclear Nonproliferation Division, Oak Ridge National Laboratory, Oak Ridge, Tennessee 37831, United States*

Jennifer L. Niedziela − *Nuclear Nonproliferation Division, Oak Ridge National Laboratory, Oak Ridge, Tennessee 37831, United States;* orcid.org/0000-0002-2990-923X

Roger J. Kapsimalis − *Nuclear Nonproliferation Division, Oak Ridge National Laboratory, Oak Ridge, Tennessee 37831, United States*

Andrew Miskowiec − *Nuclear Nonproliferation Division, Oak Ridge National Laboratory, Oak Ridge, Tennessee 37831, United States*

Complete contact information is available at: https://pubs.acs.org/10.1021/acs.inorgchem.0c01279

Notes

The authors declare no competing financial interest.

ACKNOWLEDGMENTS

The authors thank Michael Lance for his assistance in collecting IR data, David Harris and Scott Matthews for their support, and Zach Brubaker and Sara Isbill for their helpful comments. We also thank two anonymous reviewers for their careful consideration of this work, which has been significantly improved by their comments. A portion of this research was conducted at the Center for Nanophase Materials Sciences, which is a Department of Energy Office of Science User Facility. This project was supported in part by an appointment to the Science Education Programs at National Institutes of Health, administered by Oak Ridge Associated Universities through the US Department of Energy Oak Ridge Institute for Science and Education. This research used resources of the Compute and Data Environment for Science (CADES) at the Oak Ridge National Laboratory, which is supported by the Office of Science of the US Department of Energy under Contract No. DE-AC05-00OR22725. This manuscript has been authored by UT-Battelle, LLC, under contract DE-AC05-00OR22725 with the US Department of Energy (DOE). The US government retains and the publisher, by accepting the article for publication, acknowledges that the US government retains a nonexclusive, paid-up, irrevocable, worldwide license to publish or reproduce the published form of this manuscript, or allow others to do so, for US government purposes. DOE will provide public access to these results of federally sponsored research in accordance with the DOE Public Access Plan (http://energy.gov/downloads/doe-public-access-plan).

REFERENCES

(1) Schwerdt, I. J.; et al. Uranium oxide synthetic pathway discernment through thermal decomposition and morphological analysis. *Radiochim. Acta* **2019**, *107* (3), 193−205.

(2) Sweet, L. E.; et al. Investigation of the polymorphs and hydrolysis of uranium trioxide. *J. Radioanal. Nucl. Chem.* **2013**, *296* (1), 105−110.

(3) Brincat, N. A.; et al. Ab initio investigation of the UO_3 polymorphs: Structural properties and thermodynamic stability. *Inorg. Chem.* **2014**, *53* (23), 12253−12264.

(4) Shundalau, M., et al. A DFT modeling of the uranium trioxide vibration spectra characteristics. **2012**.

(5) Hoekstra, H. R.; Siegel, A. The uranium-oxygen system: U_3O_8 UO_3. *J. Inorg. Nucl. Chem.* **1961**, *18*, 154−165.

(6) Beketov, A.; Strekalovskii, V.; Vlasov, V. A study of the structure of solid solutions of uranium oxides in the range α-UO_3-U_3O_8. *J. Struct. Chem.* **1965**, *6* (1), 64−67.

(7) Sheft, I.; Fried, S.; Davidson, N. Preparation of uranium trioxide. *J. Am. Chem. Soc.* **1950**, *72* (5), 2172−2173.

(8) Palacios, M. L.; Taylor, S. H. Characterization of uranium oxides using in situ micro-Raman spectroscopy. *Appl. Spectrosc.* **2000**, *54* (9), 1372−1378.

(9) Lin, D. H. M.; et al. Applicability of Raman spectroscopy as a tool in nuclear forensics for analysis of uranium ore concentrates. *Radiochim. Acta* **2013**, *101* (12), 779−784.

(10) Schwerdt, I. J.; et al. Nuclear proliferomics: A new field of study to identify signatures of nuclear materials as demonstrated on alpha-UO3. *Talanta* **2018**, *186*, 433−444.

(11) Pointurier, F.; Marie, O. Identification of the chemical forms of uranium compounds in micrometer-size particles by means of micro-Raman spectrometry and scanning electron microscope. *Spectrochim. Acta, Part B* **2010**, *65* (9−10), 797−804.

(12) Stefaniak, E. A.; et al. Recognition of uranium oxides in soil particulate matter by means of μ-Raman spectrometry. *J. Nucl. Mater.* **2008**, *381* (3), 278−283.

(13) Sweet, L. E., et al. Spectroscopic studies of the several isomers of UO_3. in *Optics and Photonics for Counterterrorism, Crime Fighting and Defence IX; and Optical Materials and Biomaterials in Security and Defence Systems Technology X*; International Society for Optics and Photonics: 2013.

(14) El-Fekey, S. A.; et al. Solid phase decomposition of ammonium uranate. *Thermochim. Acta* **1982**, *54* (3), 327−336.

(15) Khilla, M. A.; El-Fekey, S. A.; Rofail, N. H. Infrared absorption study of uranium trioxide phases. *Radiochim. Acta* **1986**, *40* (4), 185−190.

(16) Wheeler, V.; Dell, R.; Wait, E. Uranium trioxide and the UO_3 hydrates. *J. Inorg. Nucl. Chem.* **1964**, *26* (11), 1829−1845.

(17) Sato, T.; Ozawa, F.; Shiota, S. Thermal decomposition of ammonium uranates precipitated from uranyl nitrate solution with ammonium hydroxide. *Thermochim. Acta* **1985**, *88* (1), 313−318.

(18) Kim, B. H.; et al. Thermal and X-ray diffraction analysis studies during the decomposition of ammonium uranyl nitrate. *J. Radioanal. Nucl. Chem.* **2012**, *292* (3), 1075−1083.

(19) Debets, P. C. The structure of β-UO_3. *Acta Crystallogr.* **1966**, *21* (4), 589−593.

(20) Eloirdi, R.; et al. Investigation of ammonium diuranate calcination with high-temperature X-ray diffraction. *J. Mater. Sci.* **2014**, *49* (24), 8436−8443.

(21) Cornman, W. R., Jr. *Preparation and characterization of the polymorphs of UO_3*; Du Pont de Nemours & Co. Savannah River Laboratory: Aiken, SC (United States), 1962.

(22) Katz, J. J.; Gruen, D. M. Higher oxides of the actinide elements. The preparation of Np_3O_8. *J. Am. Chem. Soc.* **1949**, *71* (6), 2106−2112.

(23) Eilers, P. H. A perfect smoother. *Anal. Chem.* **2003**, *75* (14), 3631.

(24) Sakamoto, Y.; Ishiguro, M.; Kitagawa, G. *Akaike information criterion statistics*; D. Reidel: Dordrecht, The Netherlands, 1986; p 81.

https://dx.doi.org/10.1021/acs.inorgchem.0c01279
Inorg. Chem. XXXX, XXX, XXX−XXX

(25) Kresse, G.; Furthmüller, J. Efficiency of ab-initio total energy calculations for metals and semiconductors using a plane-wave basis set. *Comput. Mater. Sci.* **1996**, *6* (1), 15−50.
(26) Kresse, G.; Furthmüller, J. Efficient iterative schemes for ab initio total-energy calculations using a plane-wave basis set. *Phys. Rev. B: Condens. Matter Mater. Phys.* **1996**, *54* (16), 11169.
(27) Kresse, G.; Hafner, J. Ab initio molecular-dynamics simulation of the liquid-metal-amorphous-semiconductor transition in germanium. *Phys. Rev. B: Condens. Matter Mater. Phys.* **1994**, *49* (20), 14251.
(28) Kresse, G.; Joubert, D. From ultrasoft pseudopotentials to the projector augmented-wave method. *Phys. Rev. B: Condens. Matter Mater. Phys.* **1999**, *59* (3), 1758.
(29) Perdew, J. P.; Burke, K.; Wang, Y. Generalized gradient approximation for the exchange-correlation hole of a many-electron system. *Phys. Rev. B: Condens. Matter Mater. Phys.* **1996**, *54* (23), 16533.
(30) Blöchl, P. E. Projector augmented-wave method. *Phys. Rev. B: Condens. Matter Mater. Phys.* **1994**, *50* (24), 17953.
(31) Dudarev, S.; et al. Electron-energy-loss spectra and the structural stability of nickel oxide: An LSDA+ U study. *Phys. Rev. B: Condens. Matter Mater. Phys.* **1998**, *57* (3), 1505.
(32) Togo, A.; Tanaka, I. First principles phonon calculations in materials science. *Scr. Mater.* **2015**, *108*, 1−5.
(33) Scherrer, P. Bestimmung der inneren Struktur und der Größe von Kolloidteilchen mittels Röntgenstrahlen. In *Kolloidchemie Ein Lehrbuch*; Springer: 1912; pp 387−409.
(34) Altomare, A.; et al. EXPO2013: a kit of tools for phasing crystal structures from powder data. *J. Appl. Crystallogr.* **2013**, *46* (4), 1231−1235.
(35) Altomare, A.; et al. New techniques for indexing: N-TREOR in EXPO. *J. Appl. Crystallogr.* **2000**, *33* (4), 1180−1186.
(36) Spek, A. L. Structure validation in chemical crystallography. *Acta Crystallogr., Sect. D: Biol. Crystallogr.* **2009**, *65* (2), 148−155.
(37) Burns, P. C.; Ewing, R. C.; Hawthorne, F. C. The crystal chemistry of hexavalent uranium: polyhedron geometries, bond-valence parameters, and polymerization of polyhedra. *Can. Mineral.* **1997**, *35*, 1551−1570.
(38) Pegg, J. T.; et al. DFT+ U study of the structures and properties of the actinide dioxides. *J. Nucl. Mater.* **2017**, *492*, 269−278.
(39) Jones, L. H. Systematics in the vibrational spectra of uranyl complexes. *Spectrochim. Acta* **1958**, *10* (4), 395−403.
(40) Bartlett, J. R.; Cooney, R. P. On the determination of uranium-oxygen bond lengths in dioxouranium (VI) compounds by Raman spectroscopy. *J. Mol. Struct.* **1989**, *193*, 295−300.
(41) Glebov, V. Electronic structure and properties of uranyl compounds. Relation between bond length and bond strength in uranyl compounds. *Koordinatsionnaya Khimiya* **1982**, *8* (7), 970−976.
(42) Momma, K.; Izumi, F. VESTA: a three-dimensional visualization system for electronic and structural analysis. *J. Appl. Crystallogr.* **2008**, *41* (3), 653−658.
(43) Allen, G. C.; Holmes, N. R. Characterization of binary uranium oxides by infrared spectroscopy. *Appl. Spectrosc.* **1994**, *48* (4), 525−530.
(44) Fodor, M.; Poko, Z.; Mink, J. Investigation of hydrolysis products from uranium trioxide and uranyl salts by derivatography and infrared spectroscopy. *Microchim. Acta* **1966**, *54* (4−5), 865−885.
(45) Tsuboi, M.; Terada, M.; Shimanouchi, T. Optically active lattice vibrations of α-uranium trioxide. *J. Chem. Phys.* **1962**, *36* (5), 1301−1310.
(46) Bullock, J. I. Raman and infrared spectroscopic studies of the uranyl ion: the symmetric stretching frequency, force constants, and bond lengths. *J. Chem. Soc. A* **1969**, 781−784.
(47) Sweet, L. E., et al. *Investigation of Uranium Polymorphs*; Pacific Northwest National Laboratory: Richland, WA (United States), 2011.
(48) Rabinowitch, E.; Belford, R. L. *Spectroscopy and photochemistry of uranyl compounds*; Pergamon: 1964; Vol. *1*.
(49) Armstrong, D.; Jarabek, R.; Fletcher, W. Micro-Raman spectroscopy of selected solid $U_xO_yF_z$ compounds. *Appl. Spectrosc.* **1989**, *43* (3), 461−468.
(50) Loopstra, B. O.; Cordfunke, E. H. P. On the structure of α-UO_3. *Recueil des Travaux Chimiques des Pays-Bas* **1966**, *85* (2), 135−142.
(51) Siegel, S.; Hoekstra, H. R. Bond lengths in gamma-uranium trioxide. *Inorg. Nucl. Chem. Lett.* **1971**, *7* (5), 455−459.
(52) Ditcham, T. G.; et al. Thermal decomposition of Australian uranium ore concentrates: characterisation of speciation and morphological changes following thermogravimetric analysis. *J. Radioanal. Nucl. Chem.* **2016**, *310* (2), 725−732.

https://dx.doi.org/10.1021/acs.inorgchem.0c01279
Inorg. Chem. XXXX, XXX, XXX−XXX